Nanoscale

Accepted Manuscript

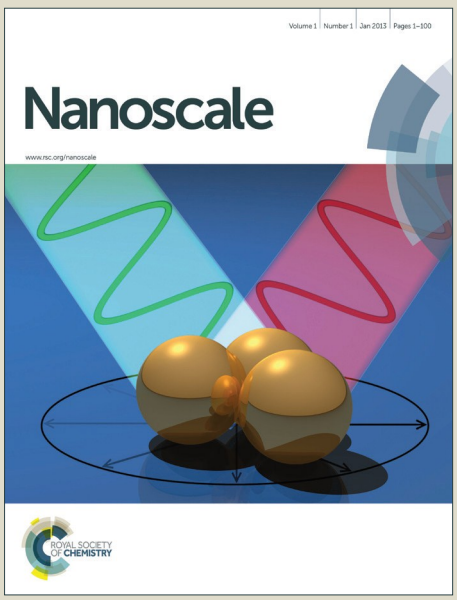

ROYAL SOCIETY OF CHEMISTRY

www.rsc.org/nanoscale

Phosphocholine-decorated Superparamagnetic Iron Oxide Nanoparticles: defining the structure and probing *in vivo* application.

Alessandra Luchini [(a,b)], Carlo Irace[(c)], Rita Santamaria[(c)], Daniela Montesarchio[(a)], Richard K. Heenan,[d] , Noemi Szekely[e] Alessandra Flori[(f)], Luca Menichetti[(f, g)], Luigi Paduano[(a,b)].*

[a] Dipartimento di Scienze Chimiche, Università degli Studi di Napoli "Federico II", Complesso Universitario di Monte S. Angelo, via Cintia, 80126 Napoli, Italy.

[b] CSGI – Consorzio interuniversitario per lo sviluppo dei Sistemi a Grande Interfase, Italy.

[c] Dipartimento di Farmacia, Università di Napoli "Federico II", Via D. Montesano 49, 80131 Napoli, Italy.

[d] ISIS Facility, Science and Technology Facilities Council, Rutherford Appleton Laboratory, Harwell Oxford, Didcot OX11 0QX, United Kingdom

[e] Jülich Centre for Neutron Science, Garching Forschungszentrum, Lichtenbergstrasse 1, D-85747 Garching bei München, Germany.

[f] Fondazione CNR/Regione Toscana G. Monaterio, Via Moruzzi, 1 I-56124, Pisa Italy

[g] CNR Institute of Clinical Physiology, Via Moruzzi, 1, I-56124, Pisa, Italy

Abstract.

Superparamagnetic Iron Oxide Nanoparticles (SPIONs) are performing contrast agents for Magnetic Resonance Imaging (MRI). A functionalization strategy of SPIONs based on hydrophobic interaction is a versatile approach easily extendable to several kind of inorganic nanoparticles and suitable to obtain stable and biocompatible systems. Here we report on the original preparation of functionalized SPIONs with 8 nm radius exploiting the hydrophobic interaction between a phosphocholine and an inner amphiphilic. With respect to other similarly functionalized SPIONs, characterized by the typical nanoparticle clustering that leads to large aggregates, our phosphocholine-decorated SPIONs are demonstrated to be monodispersed. We report the *in vitro* and *in vivo* study that proves the effective applicability of phosphocholine-decorated SPIONs as MRI contrast agents.

The versatility of this functionalization approach is highlighted by introducing on SPIONs surface a ruthenium-based potential antitumoral drug, named ToThyCholRu. Even if in this case we observed the formation of SPION clusters, ascribable to the presence of the amphiphilic ruthenium complex, interesting and promising antiproliferative activity points at the ToThyCholRu-decorated SPIONs as potential theranostic agents.

Introduction.

Functionalized Superparamagnetic Iron Oxide Nanoparticles (SPIONs) have been introduced as promising tools in the development of devices suitable for both diagnostic and therapeutic purposes.[1, 2] SPIONs are indeed able to modify the transversal proton relaxation time (T_2) of water molecules, being an effective contrast agent for Magnetic Resonance Imaging (MRI) technique.[3-6] SPIONs surface offers a valuable platform for conjugation with a large variety of molecules. Several examples of iron oxide nanoparticles functionalization are present in the literature. In these cases their surface is coated with proteins, such as albumin[7] or hemoglobin[8], surfactants[9] and oligonucleotides [10]. Suitably designed thermoresponsive polymers[11, 12], dextran[13], chitosan [14] and polyethylene glycol (PEG) [15, 16] are also commonly encountered. In particular, the nanoparticle functionalization with PEG also conjugated with other molecules such as phospholipids [17], is very popular since its approval for medical applications by the United States Food & Drug Administration (FDA) [18]. Among the inorganic nanoparticles for biomedical applications, the great success of the functionalized SPIONs, is certainly due to their recognized high biocompatibility, their simple and low cost synthesis, and the variety functionalization approaches that can be adopted to design the desired system. Furthermore, even a specific drug can be bound on the nanoparticle surface thus producing a theranostic device, which is a system able to simultaneously combine diagnosis and therapy of target pathologies. Indeed, both doxorubicin[19, 20] and cisplatin[21, 22] have been successfully bound to nanoparticles for the antitumoral therapy. However, in most cases the functionalization protocol is quite complex since it involves several steps and a large clustering of SPIONs has often been detected.

Here we report the design and preparation of small phosphocholine-functionalized SPIONs obtained through a facile functionalization protocol.[23] This functionalization strategy being very versatile, perfectly matches with the increasing interest in the development of multifunctional platforms allowing both diagnosis and therapy. Indeed, the present work took inspiration from the great results that have been already published in the SPIONs research field. [24, 25] However, our goal was the optimization of the SPIONs functionalization strategy based on hydrophobic interaction to introduce on the nanoparticle surface a widely reliable molecule, i.e. a phospholipid. In particular, we evaluated the possibility that such a simple system might be competitive with the other more sophisticated decorated-SPIONs representing at the moment the most promising systems.[25] Some examples of SPIONs functionalization realized through hydrophobic interactions are present in the literature, also including the use of phospholipids in the external coating layer. In the work by Honghong *et al.* an effective functionalization protocol to obtain SPIONs coated with two layers of

amphiphilic molecules is reported. [26] In another work by Jeon *et al.* [27], bitailed phospholipids were successfully introduced on the nanoparticle surface. However, while in the first case sodium alpha-olefin sulfate is used for SPIONs functionalization and no information about the biocompatibility of the prepared system is included, in the second work a large increment in the average size of the functionalized nanoparticles was observed. The here reported phosphocholine-decorated SPIONs represent the first example of SPIONs functionalized with a phospholipid in which both biocompatibility and small size are preserved. An effective application of the functionalized SPIONs is given by clinical MRI scanners both in water and agar gel phantoms, as well as in a murine model. The functionalized SPIONs have also been enriched by an amphiphilic ruthenium complex, named ToThyCholRu, recently synthesized and proposed for cancer therapy having high *in vitro* antiproliferative activity and lodged in the external coating layer. [28, 29] The evaluation of the bioactivity of the ToThyCholRu-functionalized SPIONs on selected human cancer and non-cancer cells confirmed the potential of the system as an effective theranostic device.

Experimental Section.

Dynamic Light Scattering (DLS)

DLS measurements were performed with a home-made instrument composed by a Photocor compact goniometer, a SMD 6000 Laser Quantum 50 mW light source operating at 5325 Å, a photomultiplier (PMT-120-OP/B) and a correlator (Flex02-01D) from *Correlator.com*. All measurements were performed at (25.00 ± 0.05) °C with temperature controlled through the use of a thermostat bath. In DLS, the intensity autocorrelation function, $g^{(2)}(t)$, is measured for the instrument configuration corresponding to the scattering angle of 90°. The intensity autocorrelation function is related to the electric field autocorrelation function, $g^{(1)}(t)$, indicated in equation q as the inverse Laplace transform of the distribution of the relaxation rate Γ used to calculate the translational diffusion coefficient $D = \Gamma/q^2$ [30]:

$$g^{(1)}(t) = \int_{-\infty}^{+\infty} \tau A(\tau) \exp\left(-\frac{t}{\tau}\right) \mathrm{d}\ln\tau \qquad (1)$$

where $\tau = 1/\Gamma$ and q is the modulus of the scattering vector $q = 4\pi n_0/\lambda \sin(\theta/2)$ $n_0 = 1.33$ is the refractive index of the solution, λ is the incident wavelength and θ represents the scattering angle. Inverse Laplace transforms were performed using a variation of CONTIN algorithm incorporated in Precision Deconvolve software[31].

For spheres diffusing in a continuum medium at infinite dilution, in the approximation of spherical objects, the diffusion coefficient is related to the hydrodynamic radius, R_h, through the Stokes–Einstein equation:

$$R_h = \frac{kT}{6\pi\eta_0 D} \quad (2)$$

where k is the Boltzmann constant, T is the absolute temperature and η_0=0.89cP is the solvent viscosity. For not spherical particles, R_h represents the radius of a spherical aggregate with the same diffusion coefficient measured. In the present system due to the high dilution it is possible to make the approximation that $\eta \cong \eta_0$, where η represents the solution viscosity. In this hypothesis, equation (2) can be reasonably used to estimate the averaged hydrodynamic radius of the particles.[30, 32]

Small Angle Neutron Scattering (SANS)

SANS measurement on 18LPC/SPIONs were performed at 25 °C with the Loq instrument located at ISIS Science and Technology Facilities Council, in Chilton (UK). The instrument is characterized by a fixed two-dimensional detector positioned at 4 metres from the sample, which can detect the positions and times of arrival of the scattered neutrons. These configuration allowed collecting data in a range of the scattering vector modulus $q = 4\pi/\lambda \sin(\theta/2)$ between 0.008 $Å^{-1}$ and 0.221 $Å^{-1}$, with θ scattering angle. The investigated systems were contained in a closed quartz cell, in order to prevent the solvent evaporation. The raw data were then corrected for background and empty cell scattering.

SANS measurement on 18LPC-ToThyCholRu/SPIONs were performed at 25 °C with the KWS2 Diffractometer operated by Julich Centre for Neutron Science at the FRMII source located at the Heinz Meier Leibtnitz Centre, Garching (Germany). Neutrons with a wavelength of 5 Angstrom and $\Delta\lambda/\lambda \leq 0.2$ were used. A two-dimensional array detector at three different wavelength (W)/collimation (C)/sample-to-detector(D) distance combinations ($W_{5Å}C_{8m}D_{2m}$, $W_{5Å}C_{8m}D_{8m}$ and $W_{5Å}C_{20m}D_{20m}$), measured neutrons scattered from the samples. These configurations allowed collecting data in a range of the scattering vector modulus q between 0.002 $Å^{-1}$ and 0.3 $Å^{-1}$.

Thus, the so obtained absolute scattering cross sections $d\Sigma/d\Omega$ data were plotted as function of q. Generally, the dependence of $d\Sigma/d\Omega$ from the scattering vector can be summarized as in equation 3.

$$\frac{d\Sigma}{d\Omega} = \phi_p V_p P(q) S(q) + bkg \quad (3)$$

where ϕ_p, $\Delta\rho$, V_p, $P(q)$, $S(q)$ represent the volume fraction of the particles, the neutron contrast, the particle volume, the form and the structure factor of the scattering particles respectively, while bkg is the incoherent and inelastic part of the scattered cross section, largely dependent on any hydrogen present.

The form factor is responsible for the shape, size, size distribution of the scattering particles, while a contribution of the structure factor can be considered when an interparticle correlation exists. The structural information contained in both the form and the structure factor can be extrapolated by choosing an appropriate model to fit the obtained experimental data.[32]

Light Microscopy

MCF-7 cells were grown on standard sterile plastic 60 mm culture dishes by plating 5 x 10^5 cells. After reaching the subconfluence, cells were incubated for 48 h with 60, 100 and 200 μM of total lipid concentration of 18LPC and 18LPC/ToThyCholRu nanoparticles under the same experimental conditions described above. Finally, cells were observed by a contrast-phase light microscope (Labovert microscope, Leizt). Microphotographs at a 200 × total magnification (20 × objective and 10 × eyepiece) were taken with a standard VCR camera (Nikon).

In vivo MRI

MRI in vivo studies were performed at 3 T using a clinical scanner (Signa HDxT, GE Healthcare, USA) equipped with a dedicated birdcage coil for small animal studies (Rapid Biomedical, Rimpar, Germany). About 0.4 mg (600 μL) of NPs previously diluted in saline solution were manually injected in bolus in the tail vein of Wistar rats (300 mg body weight). Male Wistar rats 10-12 weeks old and weighing 310 ± 3 g were used in the study: rats were anesthetized using Zoletil® + xylazine (50 and 3 mg/kg respectively).

A Fast Spin Echo sequence for T_2 mapping was applied for the acquisition with the following parameters: TR = 1000 ms; TE = 4.7 – 102.9 ms, Echo times = 8; FOV = 18x18 cm, slice thickness = 3 mm; matrix = 224x224, total acquisition time = 24 sec.

Images in coronal plane were acquired in sequence for the first 5 minutes after injection to include a few organs of interest such as liver, kidneys and myocardium. Later the acquisition was performed at increasing time intervals, up to 60 minutes after the injection. A ROI was selected on the image

relative to the anatomical district of interest and the corresponding T_2 was assessed for each acquisition; the transverse relaxation rate (R_2) was estimated as the inverse of T_2.

Experiments with animals were performed after approval by the dedicated Committee designed by the Board of the Centre for Experimental Biology at the CNR Research Area (Pisa) and were authorised by the Italian Ministry of Health according to current national legislation (dlg26 / 2014). The Design and Realization of the project has been guided by the respect of European guidelines with particular reference to the principle of the "*three R*" and ethical use of animals.

Results and Discussions.

Preparation and Characterization the functionalized SPIONs.

Assessing the full stability and biocompatibility of a system under investigation for biomedical applications is a mandatory task. SPIONs with 3 nm radius, as estimated from SAXS measurement, have been synthesized through thermal decomposition method [33] with a first coating layer composed by oleic acid and oleylamine molecules. The size of the SPIONs together with the first coating layer were evaluated by means of DLS, as corresponding to an hydrodynamic radius of 6 nm (for the obtained SPIONs synthesis and characterization see the Supporting Information).

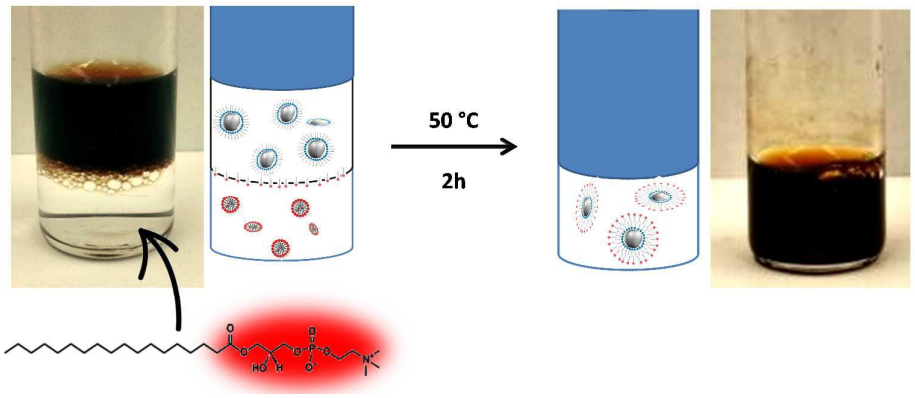

Figure 1: *The synthesized SPIONs are stable in non-polar solvent, such as cyclohexane, due to their oleic acid and oleylamine coating. The organic solvent suspension has been layered on top of a 18LPC water solution. In the water phase, the 18LPC is shared between micelle aggregates and a layer at interphase. As the cyclohexane evaporate the nanoparticles concentrate at interphase and through the 18LPC decoration they dissolve in water. The final result is a homogeneous water solution, in which the 18LPC-functionalized SPIONs with a single sharp size distribution are stably dispersed.*

The functionalization strategy exploits the hydrophobic tails of oleic acid and oleylamine molecules, which are bound to the nanoparticle surface, to introduce a second layer of biocompatible amphiphilic molecules. In the present case the 1-octadecyl-2-hydroxy-*sn*-glycero-3-

phosphocholine (18LPC) was used (Figure 1). The structure of the second layer is such that amphiphilic molecules polar heads are oriented toward the solvent, thus allowing high water stability.

In detail, the synthesized SPIONs suspension in cyclohexane has been stratified over an aqueous solution containing 18LPC at $4 \cdot 10^{-2}$ molal concentration. Bath sonication of the biphasic system at 50 °C for about 2 h promoted the cyclohexane evaporation and the transfer into the aqueous phase of the SPIONs coated with the second layer of 18LPC, named 18LPC/SPIONs.

The same procedure has been used to prepare the functionalized SPIONs in which the ToThyCholRu is included in the outer layer, named 18LPC-ToThyCholRu/SPIONs. A solution of 18LPC and ToThyCholRu with respectively 90/10 molar ratio and total concentration $4 \cdot 10^{-2}$ molal has been prepared and used to functionalize the synthesized SPIONs as previously described in the case of pure 18LPC solution. The percentage of ToThyCholRu has been chosen on the basis of previous experiments.[29]

The 18LPC/SPIONs suspension was characterized combining DLS and SANS measurements. In particular, DLS measurements can be used to evaluate the number of scattering populations present within the suspension and their mean hydrodynamic radius (R_h). As reported in the equation 2, R_h is calculated from the diffusion coefficient of the scattering particle and thus by definition it takes into account of both the particle size and the solvation shells that diffuse with it. On the other hand, SANS data were analyzed to gain more details on the structure of the scattering particles. It is worth to note that the radius estimated from SANS data, is smaller if compared to the R_h, since it does not consider all the solvation shells around the particle.

From the DLS data, 18LPC/SPIONs resulted to have a mean R_h of about 8 nm (figure 2). The estimated value of the hydrodynamic radius is slightly larger than the one of the non-functionalized SPIONs, (about 6 nm). Considering the length of the 18LPC molecules, the obtained R_h is reasonably compatible with the formation of a second amphiphilic layer on SPIONs surface. SANS experiment aimed to define the structure of both the inorganic and the organic components of the functionalized SPIONs. The experimental data were treated, according to equation 4, as arising from a population of non-interacting spherical nanoparticles having a core-shell structure. In particular, the 18LPC/SPIONs core is composed by the Fe_3O_4 iron oxide, while the organic shell includes the two amphiphilic layers.

$$P_{core\text{-}shell}(q) = \frac{1}{V^2}\left[3V_{core}\left(\rho_{core} - \rho_{shell}\right)\frac{\left[sin\left(qr_{core}\right) - qr_{core}cos\left(qr_{core}\right)\right]}{\left(qr_{core}\right)^3} + 3V_{shell}\left(\rho_{shell} - \rho_{D_2O}\right)\frac{\left[sin\left(qr_{shell}\right) - qr_{shell}cos\left(qr_{shell}\right)\right]}{\left(qr_{shell}\right)^3} \right]^2 \quad (4)$$

In the model the following scattering length density calculated considering the atomic compositions and the molecular volumes were used: $\rho_{Fe_3O_4}^{neutron} = 6.9 \cdot 10^{-6}\text{Å}^{-2}$(core), $\rho_{oleic\ acid}^{neutron} = 7.8 \cdot 10^{-8}\text{Å}^{-2}$ (inner layer), $\rho_{oleylamine}^{neutron} = -1.7 \cdot 10^{-7}\text{Å}^{-2}$(inner layer), $\rho_{18LPC}^{neutron} = 2.9 \cdot 10^{-7}\text{Å}^{-2}$ (outer layer) and $\rho_{D_2O}^{neutron} = 6.3 \cdot 10^{-6}\text{Å}^{-2}$. Taking into account the composition of the organic shell, made out of the inner layer of oleic acid and oleylamine molecules (50/50 mol/mol) and the 18LPC outer layer, its scattering length density was estimated as corresponding to $0.62 \cdot 10^{-6}\text{Å}^{-2}$.

The very good agreement between the experimental data and the fitting model confirmed the obtainment of functionalized SPIONs with core-shell structure. In particular, core radius value of about 3 nm perfectly matches the one evaluated for the SPIONs (in cyclohexane suspension) through the SAXS measurements (see Table 1 and ESI). Furthermore, the estimated shell thickness of about 4 nm is comparable with the summed length of the oleic acid and oleylamine molecules (inner layer) and the 18LPC molecule (outer layer). This seems to confirm that indeed two layers of amphiphilic molecules are present on the SPIONs surface.

Considering the differences in the meaning of the R_h and the SPIONs radius estimated by SANS experiments, the overall SPIONs size, including both the core radius and the organic shell thickness, is in agreement with the hydrodynamic radius resulted from the DLS measurements, if the hydration of the outer organic shell is taken into account.

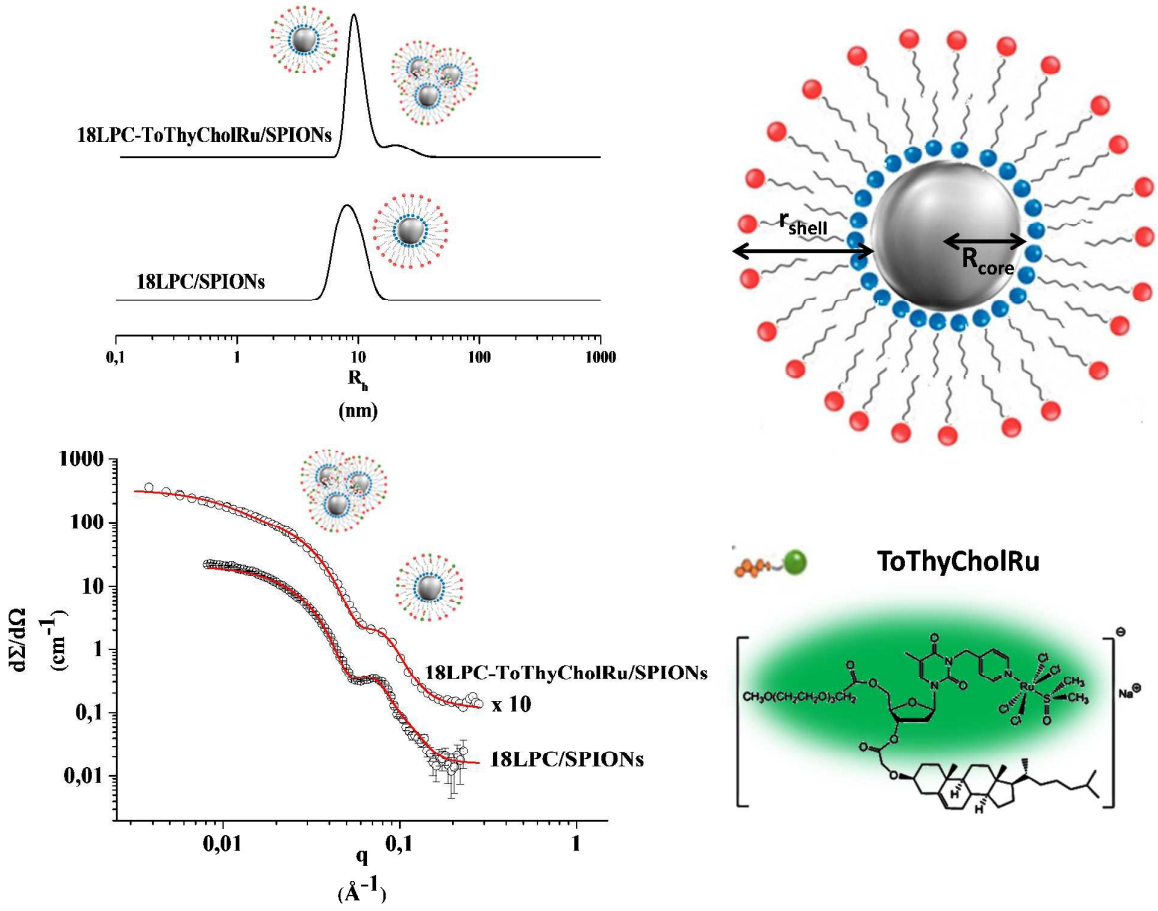

Figure 2: *DLS and SANS data collected for both 18LPC/SPIONs and 18LPC-ToThyCholRu/SPIONs (left). Schematic representation of functionalized SPIONs highlighting its core-shell structure together with ToThyCholRu structure (right).*

18LPC/SPIONs				
R_h (nm)		**r_{core} (nm)**		**r_{shell} (nm)**
(8 ± 2)		(3.2 ± 0.1)		(3.8 ± 0.3)
ToThyCholRu-18LPC/SPIONs				
R_h (MNPs) (nm)	**R_h (Cluster) (nm)**	**r_{core} (nm)**	**r_{shell} (nm)**	**$r_{cluster}$ (nm)**
(11 ± 1)	(30 ± 3)	(2.7 ± 0.5)	(3.7 ± 0.4)	(20 ± 1)

Table 1: *Structural parameters of both 18LPC/SPIONs and 18LPC-ToThyCholRu/SPIONs obtained from DLS and SANS data.*

The same characterization based on combining DLS and SANS results was also performed on ToThyCholRu-18LPC/SPIONs suspension. As it is shown from the R_h distribution reported in figure 2, two populations were present within the sample. Furthermore, also the analysis of the

SANS data (Figure 2) indicated that the core-shell form factor used for 18LPC/SPIONs was not sufficient, to fully reproduce the experimental data. In order to interpret these results, it has to be considered that ToThyCholRu structure, reported in figure 2, is very different from 18LPC one. Indeed, it can be demonstrated by calculations of the molecular volumes that ToThyCholRu polar head (highlighted in green in Figure 2) is about four times larger than 18LPC polar head. Taking into account these structural differences, it reasonable to assume that ToThyCholRu is less efficient in guaranteeing SPION coating with respect to 18LPC, and thus cluster formation resulted to be prometed (see detailed discussion in the ESI).

Considering the coexistence of single functionalized nanoparticles, presenting structural characteristics close to the 18LPC/SPIONs, together with small clusters, SANS data were analyzed according to equation 5.

$$I(q)=\varphi_{core\text{-}shell}\ V_{core-shell}P_{core\text{-}shell}+\varphi_{cluster}V_{cluster}P_{cluster}+Bkg \quad (5)$$

with

$$P_{core-shell}(q)=\frac{1}{V^2}\left[3V_c(\rho_c-\rho_s)\frac{\sin(qr_c)-qr_c\cos(qr_c)}{qr_c}+3V_s(\rho_s-\rho_{solv})\frac{\sin(qr_s)-qr_s\cos(qr_s)}{qr_s}\right]^2$$

and

$$P_{cluster}(q)=\frac{1}{V^2}\left[3V_{cluster}(\rho_{cluster}-\rho_{solv})\frac{\sin qr_{cluster}-qr_{cluster}\cos(qr_{cluster})}{qr_{cluster}}\right]^2$$

The scattered intensity was considered as arising from a population of functionalized SPIONs with core-shell structure and a population of nanoparticle clusters treated as a homogenous sphere. The structural parameters that led to the best fit of the experimental data are reported in table 1. The nanoparticles clusters present in the 18LPC-ToThyCholRu/SPIONs can be reasonably considered spherical, as verified by Cryo-Transmission Electron Miscroscopy (Cryo-TEM) images (see ESI). The clusters are composed by the iron oxide cores and organic molecules, which will be exposed on the cluster surface, but still present also in the cluster core. Indeed, it is reasonable to assume that the iron oxide cores being coated by the oleic acid and oleylamine molecules, are stuck together through hydrophobic interaction. According to this cluster structure, it is no longer possible to identify an inorganic core and an organic shell. Thus the clusters were treated as homogenous sphere, having a scattering length density calculated as the average of the scattering length densities of each components according to their composition and volume fraction. The very good agreement obtained between the experimental data and the fitting curve built according to the described model confirmed the interpretation of the ToThyCholRu-18LPC/SPION suspension as composed by both single functionalized nanoparticles and small clusters with sizes less than 100nm. Furthermore, as

evaluated from SANS data analysis the volume fraction of clusters corresponds to the 20% of the total suspension volume, while the fraction of clusters with respect to the total particle number present in the sample, estimated from DLS data, corresponds to 5%.

The main advantage of the proposed functionalization strategy is certainly its simplicity and the reliability of the major component used for decorating the SPIONs, i.e. 18LPC. Functionalized SPIONs are obtained with low increment in terms of size and no further purification step is required. Indeed, 18LPC/SPIONs were demonstrated to be monodispersed, while a small fraction of clusters together with single functionalized nanoparticles are observed in case of ToThyCholRu-18LPC/SPIONS.

18LPC/SPIONs and 18LPC-ToThyCholRu/SPIONs in vitro bioscreens.

Preliminary *in vitro* investigations are fundamental to verify the effective biocompatibility and to ensure the theoretical safety towards biological environment of the functionalized SPIONs, thereby allowing for their potential *in vivo* use. According to our experimental procedures, the performed bioscreens are based on the estimation of a ‘‘cell survival index’’ deriving concurrently from the evaluation of the cellular metabolic activity (MTT colorimetric assay) and the determination of live/dead cells ratio (TC20 automated cell counter), as reported in the ESI.

The results emerging from a selected panel of cultured tumor and non-tumor cell lines provide evidence for very interesting patterns, showing 18LPC/SPIONs devoid of significant biological effects even at the higher iron concentration of 100 μg/ml (cell survival index always higher than 80% in bioscreens, see ESI for details). This outcome is an excellent starting point in the design of effective SPIONs-based MRI contrast agents as well as of effective nanoplatforms for theranostics.

Conversely, the presence of the amphiphilic ruthenium complex ToThyCholRu on the SPIONs surface induced a significantly enhanced bioactivity, providing relevant concentration-dependent cytotoxic responses in the human cancer cells of different histological origin and endowed with high replicative potential *in vitro.* To support the relationship between cell viability and ruthenium-induced cytotoxicity, subconfluent cultures cells were examined by phase-contrast light microscopy for the dynamic cell population monitoring of the morphological changes that occur during cell death. As shown in Figure 4, *in vitro* exposure to 18LPC/SPIONs does not cause substantial cytologic changes, whereas after 18LPC-ToThyCholRu/SPIONs application some morphological modifications of the cell monolayers clearly appear. Microscopy images provide evidence that the reduction in cell viability is exclusively correlated to the presence of the active ruthenium and is thereby associated with well detectable dose-dependent cytotoxic effects.

18LPC/SPIONs are completely free of macroscopic biological effects on healthy cultured cells. On the other hand, 18LPC-ToThyCholRu/SPIONs show relevant cytotoxicity selectively *versus* human cancer cells, thereby fully supporting their use as theranostic devices.

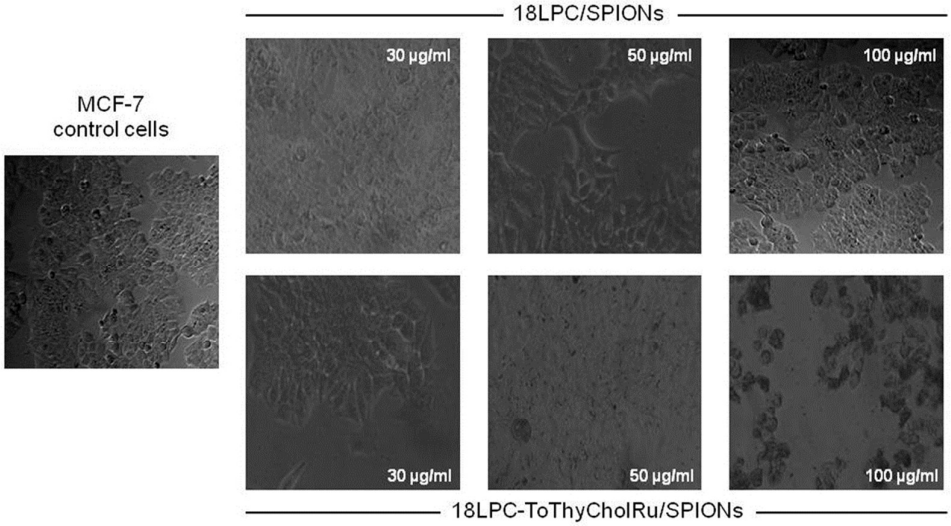

Figure 4:*Representative microphotographs at a 200 × magnification (20 × objective and a 10 × eyepiece) by phase-contrast light microscopy of MCF-7 cells lines untreated (control cells) or treated for 48 h with the indicated iron concentration of 18LPC/SPIONs (top line) and of 18LPC-ToThyCholRu/SPIONs (bottom line). For the latter, the corresponding ruthenium concentrations are 6, 10 and 20 µM, respectively. The shown images are representative of three independent experiments.*

MRI Measurements.

Having proved their high biocompatibility, the 18LPC/SPIONs were injected in a small animal model (healthy rat) to test *in vivo* their pharmacokinetics and the extent of the negative contrast associated to the transverse proton relaxation time (T_2) reduction. A major effect on T_2 relaxation time was recorded in the liver of the animal (for both right and left side), which is consistent with the 18LPC/SPIONs fate, being mainly sequestered by the reticuloendothelial hepatic tissue (Kupffer cells).[34, 35] In particular, an increase of the transverse proton relaxation rate (R_2) value was already observed 10 minutes after the injection, reaching a maximum after 60 minutes, in agreement with a progressive accumulation of the 18LPC/SPIONs in the tissue for excretion (Figure 5). Conversely, we did not detect a significant variation of R_2 over time in other organs such as the kidneys or the heart. Thus, the map of relaxation rate demonstrated an efficient effect *in vivo*, which is promising for future applications in targeted therapies.

The progressive increase of the transverse relaxation rate (R_2) detected over time for a *Region Of Interest* (ROI) selected in the right hepatic lobe is in good agreement with previous findings obtained for clinically used ultra-small superparamagnetic iron oxide nanoparticles (USPIONs), that are typically recognized by the reticuloendothelial system. The 18LPC/SPIONs demonstrated a measurable reduction in the MR signals in the rat liver after injection, indicating that they have potential for use as T_2 MRI (negative) contrast agents with significant enhanced sensitivity and a suitable blood-half life.

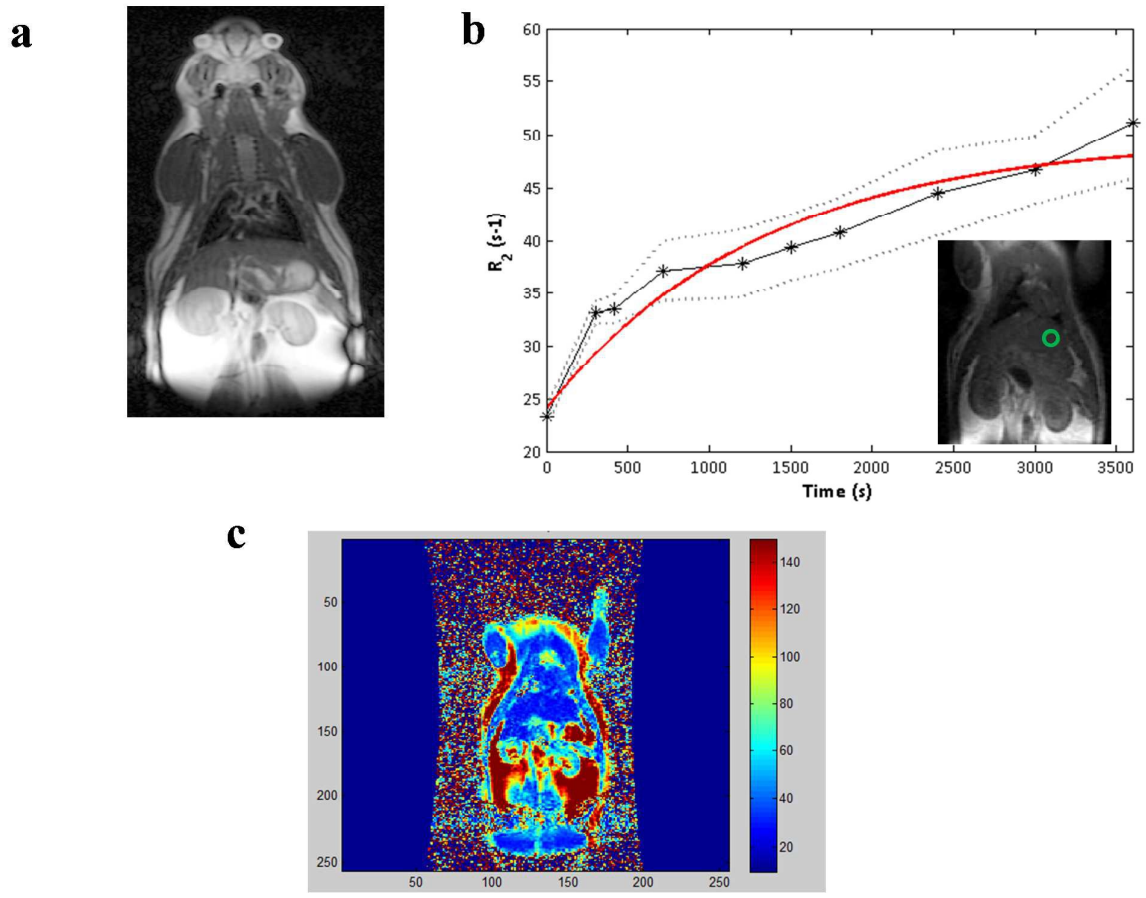

Figure 5: *T_2-weighted image of a coronal view of the animal (Wistar rat) before injection of the 18LPC/SPIONs (panel a) Transverse relaxation rate ($R_2=1/T_2$, s^{-1}) measured after bolus injection of 1,7 μg/g in the tail vein of 18LPC/SPIONs in 0.9% NaCl solution(panel b). The corresponding ROI (see insert in panel b) was selected in the coronal plane covering the liver: mean±SE indicated by the gray intervals;. Representative T_2-mapping MRI image of a coronal view after injection (t=3 min) of the 18LPC/SPIONs (panel c)*

Conclusions

The design, preparation and characterization of biocompatible phosphocholine-decorated SPIONs as effective nano-platforms for the development of theranostic devices are here described.

During the last 10 years great efforts have been made in the synthesis and functionalization of iron oxide nanoparticles for their applications as theranostic agents. Indeed, important results have already been achieved, and many examples of performing and promising functionalized SPIONs can be found in the literature. Here we have reported a further implementation of SPIONs functionalization through hydrophobic interaction based on the use of simple and highly reliable molecules, i.e. phospholipids. This work was inspired by the major results that the research in the SPIONs field have achieved within the last years. Our contribution might be seen as the application of these results for optimizing the preparation of performing functionalized SPIONs. Indeed, we have demonstrated through a complete physico-chemical characterization based on the combined use of several scattering techniques, the obtainment of phosphocholine-functionalized SPIONs, representing the smallest example of SPIONs functionalized with a phospholipid, in which the biocompatibility is retained. The phosphocholine-functionalized SPIONs, owing to the small dimension, favourable long circulation and enhanced MRI T_2, have been proved to be performing contrast agents. Furthermore, the versatility of the presented SPIONs functionalization strategy was showed by successfully introducing on SPIONs surface the ruthenium complex ToThyCholRu. As demonstrated by the *in vitro* bioscreens the 18LPC-ToThyCholRu/SPIONs have high potential for the simultaneous detection and therapy of cancer.

We believe that the present work demonstrates the possibility of obtaining performing functionalized SPIONs as MRI contrast agents, without the need of using complex functionalizing agents. Furthermore it does contains useful structural information about the functionalized SPIONs that might be relevant for the researcher that are already working in this field and for those who are at the moment approaching these kind of systems.

Acknowledgements

We thank MIUR (PRIN 2010-BJ23MN_007) for financial support, the Julich center for neutron science (JCNS) and ISIS at the STFC Rutherford Appleton Laboratory for providing the beam time

References

1. K. Tomankova, K. Polakova, K. Pizova, S. Binder, M. Havrdova, M. Kolarova, E. Kriegova, J. Zapletalova, L. Malina, J. Horakova, J. Malohlava, A. Kolokithas-Ntoukas, A. Bakandritsos, H. Kolarova and R. Zboril, *Int J Nanomed*, 2015, **10**, 949-961.
2. M. Mahmoudi, S. Sant, B. Wang, S. Laurent and T. Sen, *Advanced Drug Delivery Reviews*, 2011, **63**, 24-46.
3. O. Bomati-Miguel, N. Miguel-Sancho, I. Abasolo, A. P. Candiota, A. G. Roca, M. Acosta, S. Schwartz, C. Arus, C. Marquina, G. Martinez and J. Santamaria, *J Nanopart Res*, 2014, **16**, 1-13.
4. F. Y. Dai, M. H. Du, Y. G. Liu, G. Y. Liu, Q. J. Liu and X. Zhang, *J Mater Chem B*, 2014, **2**, 2240-2247.

5. K. Abbas, F. Simonelli, U. Holzwarth, I. Cydzik, A. Bulgheroni, N. Gibson and J. Kozempel, *Applied radiation and isotopes : including data, instrumentation and methods for use in agriculture, industry and medicine*, 2013, **73**, 44-48.
6. S. V. E. Laurent, Luce; , *Chemistry of Contrast Agents in Medical Magnetic Resonance Imaging (2nd Edition)*, 2013, 427-447.
7. T. V. V. Thao Truong-Dinh Tran∗, Phuong Ha-Lien Tran, *Chemical Engineering Research and Design*, 2015, **9**, 112-118.
8. M. O. Esra Maltas *Materials Science and Engineering C*, 2015, **54**, 43-49.
9. R. K. Kishore Kumar Nair, Nusrat Iqbal, Abshar Hasan, Samsul Alam and SKRaza, *Materials Research Express*, 2015, **2**.
10. E. E. White, A. Pai, Y. M. Weng, A. K. Suresh, D. Van Haute, T. Pailevanian, D. Alizadeh, A. Hajimiri, B. Badie and J. M. Berlin, *Nanoscale*, 2015, **7**, 7780-7789.
11. M. Rahman, Y. Nahar, W. Ullah, A. Elaissari and H. Ahmad, *J Polym Res*, 2015, **22**, 1-9.
12. M. Chiper, K. H. Aubert, A. Auge, J. F. Fouquenet, M. Souce and I. Chourpa, *Nanotechnology*, 2013, **24**.
13. H. Hauser and P. Fulmek, *Ieee T Magn*, 1992, **28**, 1815-1825.
14. D. Bhattacharya, S. K. Sahu, I. Banerjee, M. Das, D. Mishra, T. K. Maiti and P. Pramanik, *J Nanopart Res*, 2011, **13**, 4173-4188.
15. A. P. Khandhar, R. M. Ferguson, H. Arami, S. J. Kemp and K. M. Krishnan, *Ieee T Magn*, 2015, **51**.
16. V. Pourcelle, S. Laurent, A. Welle, N. Vriamont, D. Stanicki, L. Vander Elst, R. N. Muller and J. Marchand-Brynaert, *Bioconjugate chemistry*, 2015, **26**, 822-829.
17. E. V. Shtykova, X. L. Huang, N. Remmes, D. Baxter, B. Stein, B. Dragnea, D. I. Svergun and L. M. Bronstein, *J Phys Chem C*, 2007, **111**, 18078-18086.
18. D. Ling, N. Lee and T. Hyeon, *Accounts of chemical research*, 2015, **48**, 1276-1285.
19. J. Gautier, E. Allard-Vannier, J. Burlaud-Gaillard, J. Domenech and I. Chourpa, *J Biomed Nanotechnol*, 2015, **11**, 177-189.
20. M. Halupka-Bryl, K. Asai, S. Thangavel, M. Bednarowicz, R. Krzyminiewski and Y. Nagasaki, *Colloids and surfaces. B, Biointerfaces*, 2014, **118**, 140-147.
21. C. S. Chiang, Y. H. Tseng, B. J. Liao and S. Y. Chen, *Advanced healthcare materials*, 2015, **4**, 1066-1075.
22. H. Unterweger, R. Tietze, C. Janko, J. Zaloga, S. Lyer, S. Durr, N. Taccardi, O. M. Goudouri, A. Hoppe, D. Eberbeck, D. W. Schubert, A. R. Boccaccini and C. Alexiou, *Int J Nanomedicine*, 2014, **9**, 3659-3676.
23. A. Luchini, G. Vitiello, F. Rossi, O. R. De Ballesteros, A. Radulescu, G. D'Errico, D. Montesarchio, C. D. Fernandez and L. Paduano, *Phys Chem Chem Phys*, 2015, **17**, 6087-6097.
24. E. K. Lim, T. Kim, S. Paik, S. Haam, Y. M. Huh and K. Lee, *Chemical reviews*, 2015, **115**, 327-394.
25. N. Lee, D. Yoo, D. Ling, M. H. Cho, T. Hyeon and J. Cheon, *Chemical reviews*, 2015, **115**, 10637-10689.
26. L. Q. Honghong Li, Ying Feng, Lihua Hu, Chunhua Zhou, *J Magn Magn Mater*, 2015, **384**, 213-218.
27. S. L. Jeon, M. K. Chae, E. J. Jang and C. Lee, *Chem-Eur J*, 2013, **19**, 4217-4222.
28. L. Simeone, G. Mangiapia, G. Vitiello, C. Irace, A. Colonna, O. Ortona, D. Montesarchio and L. Paduano, *Bioconjugate chemistry*, 2012, **23**, 758-770.
29. G. Vitiello, A. Luchini, G. D'Errico, R. Santamaria, A. Capuozzo, C. Irace, D. Montesarchio and L. Paduano, *J Mater Chem B*, 2015, **3**, 3011-3023.
30. B. J. B. a. R. Pecora, *Dynamic Light Scattering: With Applications to Chemistry, Biology, and Physics* Couvire Dover Publications, 2003.
31. A. Lomakin, D. Teplow and G. Benedek, in *Amyloid Proteins*, ed. E. Sigurdsson, Humana Press, 2005, vol. 299, ch. 10, pp. 153-174.
32. J. S. H. a. H. C. Benoit, *Polymers and Neutron Scattering*, Clarendon Press, 1997.
33. S. Sun, H. Zeng, D. B. Robinson, S. Raoux, P. M. Rice, S. X. Wang and G. Li, *J Am Chem Soc*, 2004, **126**, 273-279.
34. A. Tanimoto, K. Oshio, M. Suematsu, D. Pouliquen and D. D. Stark, *Journal of Magnetic Resonance Imaging*, 2001, **14**, 72-77.

35. A. Boni, G. Bardi, A. Bertero, V. Cappello, M. Emdin, A. Flori, M. Gemmi, C. Innocenti, L. Menichetti, C. Sangregorio, S. Villa and V. Piazza, *Nanoscale*, 2015, **7**, 7307-7317.

Graphical Abstract: